Intruder excitations in ^{35}P

M. Wiedeking,[1,2] E. Rodriguez-Vieitez,[1,3] P. Fallon,[1] M. P. Carpenter,[4] R. M. Clark,[1] D. Cline,[5] M. Cromaz,[1] M. Descovich,[1] R. V. F. Janssens,[4] I.-Y. Lee,[1] M.-A. Deleplanque,[1] A. O. Macchiavelli,[1] F. S. Stephens,[1] R. Teng,[5] X. Wang,[4] D. Ward,[1] C. Y. Wu,[2] S. Zhu,[4] T. Otsuka,[6,7] Y. Utsuno,[8] and A. Volya[9]

[1]*Lawrence Berkeley National Laboratory, Berkeley, California 94720, USA*
[2]*Lawrence Livermore National Laboratory, Livermore, California 94550, USA*
[3]*University of California, Berkeley, California 94720, USA*
[4]*Argonne National Laboratory, Argonne, Illinois 60439, USA*
[5]*University of Rochester, Rochester, New York 14627, USA*
[6]*University of Tokyo, Hongo, Tokyo 113-0033, Japan*
[7]*RIKEN, Hirosawa, Wako-shi, Saitama 351-0198, Japan*
[8]*Japan Atomic Energy Agency, Tokai, Ibaraki 319-1195, Japan*
[9]*Florida State University, Tallahassee, Florida 32306, USA*

(Received 21 April 2008; revised manuscript received 1 August 2008; published 17 September 2008)

The structure of the neutron-rich $N = 20$ nucleus ^{35}P has been investigated through nucleon transfer experiments using the ^{208}Pb(^{36}, $X\gamma$) reaction at 230 MeV. The level structure, of mainly $1\hbar\omega$ excitations in ^{35}P, has been significantly expanded. The measurements are compared with shell model calculations. Experimental branching ratio limits are reported for predicted transitions to the $2\hbar\omega$ bandheads in ^{35}P and ^{34}Si.

DOI: 10.1103/PhysRevC.78.037302 PACS number(s): 21.10.−k, 23.20.Lv, 25.70.Hi, 27.30.+t

The shell structure of exotic nuclei and its evolution with increasing neutron-proton asymmetry is a major research topic in nuclear structure physics [1]. At β stability, the $N = Z = 20$ shell closures are large, and ^{40}Ca is a doubly magic spherical nucleus. Remove protons and the neutron-rich nuclei ^{32}Mg [2–4], ^{31}Na, [5,6], and ^{30}Ne [7], despite being located at $N = 20$, are now characterized by well-deformed intruder ground states corresponding to particle-hole (predominantly $2\hbar\omega$) excitations across the $N = 20$ shell gap from the sd to pf shell [8]. This onset of deformation (referred to as the island of inversion) has been linked to a reduction in the $N = 20$ shell gap ([9,10]) due to the influence of the strong $V_{\sigma\tau}$ neutron-proton spin-isospin interaction on the effective single-particle energies (s.p.e.) [11]. While particle-hole sd-pf cross-shell intruder configurations are the ground state within the island of inversion, they exist as excited states in heavier $N = 20$ nuclei ($Z > 12$). The excitation energy of intruder states (specifically the $2\hbar\omega$ bandhead) as a function of Z along $N = 20$ provides information on the evolution of the sd-pf shell gap and on the strength of the $V_{\sigma\tau}$ residual interaction as well as nucleon (particle-hole and particle-particle) correlations. The location of these intruder states is an important test for shell model calculations and their capability to describe cross-shell excitations and collective phenomena. The $2\hbar\omega$ deformed intruder state bandhead has been observed at an excitation energy of 3346(4) keV in ^{36}S [12], but not in ^{35}P or ^{34}Si despite significant efforts in ^{34}Si [13–16]. In ^{33}Al, a candidate $2\hbar\omega$ excitation has been reported at 730 keV [13].

We report on experiments that study excited intruder states and their decay properties in ^{35}P and ^{34}Si using deep-inelastic/transfer reactions and compare these results to shell model calculations.

Two complementary experiments were performed at the Argonne Tandem-Linac Accelerator System (ATLAS) to populate neutron-rich $A \sim 35$ nuclei utilizing the reaction ^{208}Pb(^{36}S, $X\gamma$) at 230 MeV. The first experiment of 6.5 days was performed with an average beam current of ∼1.5 pnA, on a "thin" 0.5 mg/cm^2 target. Binary transfer products were detected using the forward half of the heavy-ion parallel-plate avalanche counter (PPAC) array CHICO [17] with an active polar-angle range of 12° to 85° relative to the beam. The compact heavy-ion counter (CHICO) differentiates target-like and projectile-like reaction products by time-of-flight differences with a resolution of ∼0.7 ns. Polar θ and azimuthal ϕ angular information is available with resolutions of $\delta\theta \sim 1°$ and $\delta\phi \sim 4.7°$, respectively. The online trigger required simultaneous detection of both reaction products in CHICO together with a γ-ray multiplicity of $\geqslant 2$ detected with Gammasphere [18], consisting of 101 high-purity (HP) Ge detectors. Event-by-event Doppler-shift reconstruction of the γ rays was applied using the scattering angles θ and ϕ and the velocities of the reaction products. The differentiation of the beam-like and target-like particles, together with gated γ transitions, produced clean spectra from which transitions were unambiguously assigned to a particular nucleus. The recoil velocity of $\beta \sim 0.1c$ for the beam-like products gives a full width at half maximum (FWHM) of ∼10 keV for γ rays at 1 MeV.

For the second experiment, a ∼0.3 pnA beam incident on a "thick" 44 mg/cm^2 ^{208}Pb target was used for 2.5 days. Reaction products were stopped within the target, and γ decay from states with lifetimes longer than the stopping time (∼1 ps) were emitted from nuclei at rest giving a FWHM of 2–3 keV for 1 MeV γ transitions. This improved the identification of weaker transitions. The hardware trigger required a γ-ray multiplicity of $\geqslant 3$ detected with Gammasphere consisting of 95 HPGe detectors. In addition to prompt γ radiation, both experiments were sensitive to isomeric decays in the time window of two beam pulses, which were 820 ns apart.

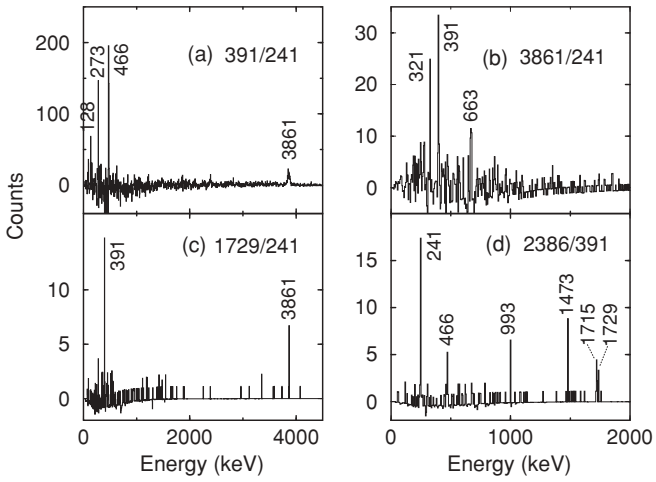

FIG. 1. Typical γ-ray spectra obtained from the thin-target Gammasphere-CHICO experiment in (a) and (b) and from the thick-target Gammasphere experiment in (c) and (d) (see text for details). Transitions associated with decays from ^{35}P are labeled by their energies.

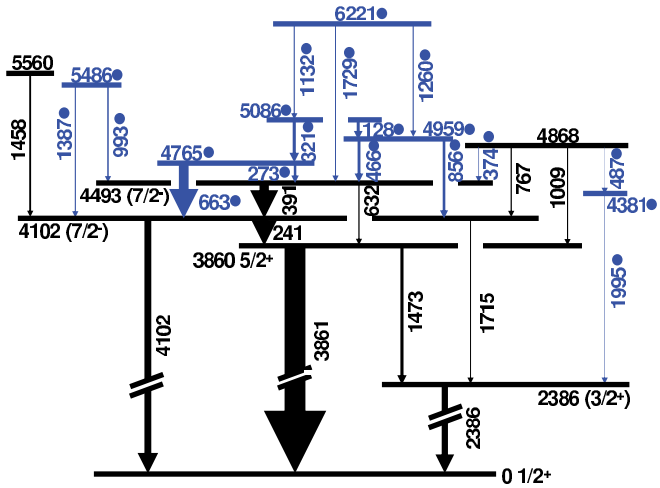

FIG. 2. (Color online) ^{35}P transitions and states observed in this work. Those in black (not marked by filled circles) have been reported previously [19–22]. Those in blue (filled circles) are new additions from this work. The states at 6221, 5560, 5486, 4868, and 4381 keV were observed only in the thick-target measurement. The width of the transitions are an indication of their relative intensities normalized to the 3861 keV transition.

Data were sorted into triple γ-coincidence "cubes." Representative ^{35}P γ-ray spectra from both experiments, gated on two γ lines, are shown in Fig. 1. Spectra gated on the prompt time peak and the beam-like particles from the Gammasphere-CHICO experiment are provided in Figs. 1(a) and 1(b). Spectra from the thick-target data gated on the off-prompt region between two beam pulses (820 ns apart) are shown in Figs. 1(c) and 1(d), and they enhance the weaker transitions fed by longer-lived states or populated in β decay. The greater sensitivity to weak transitions due to the better resolution is apparent, but no additional prompt γ rays were observed in ^{35}P from the thick-target data.

The level scheme established in this work is presented in Fig. 2. Transitions and states shown in black (those not marked by filled circles) have been observed previously [19–22]. The 1995 keV γ ray had been observed [22], but was not placed in the level scheme. From our data, it can be placed and deexcites the new level at 4381 keV. Newly observed transitions (marked by filled circles) originate from levels between 4.3 and 6.3 MeV in excitation energy. Unfortunately, their low intensity does not allow a reliable angular distribution measurement. Thirteen new γ transitions and 6 new states were assigned to ^{35}P. The uncertainty in the observed γ-ray energies is $\sim$1 keV.

The ^{34}Si channel was also populated in both data sets. Although the previously reported transitions at 3326, 930, 4255, 125, and 591 keV [14–16,23] were clearly observed, no additional information could be extracted.

Reproducing the experimental data is a key step in validating model calculations. In Fig. 3, ^{35}P experimental states are compared with the m-scheme models, continuum shell model (CoSMo), and Monte Carlo shell model (MCSM). On the left side of this figure, all known states (from this and previous works) are given. A relatively high density of states is observed for excitation energies between 4.5 and 5.5 MeV. Spin and parity information is available for the states 5197 keV $5/2^+$, 4665 keV $5/2^+$, 4493 keV $(7/2^-)$, 4102 keV $(7/2^-)$, 3860 keV $5/2^+$, 2386 keV $3/2^+$, and the ground state with $1/2^+$ from Refs. [20,21,24]. The measured positive-parity states in ^{35}P are shown by dashed-dotted black lines ($0\hbar\omega$ or $2\hbar\omega$), the tentatively assigned negative-parity states ($1\hbar\omega$) by solid green lines, and states of unknown spin and parity by dashed brown lines.

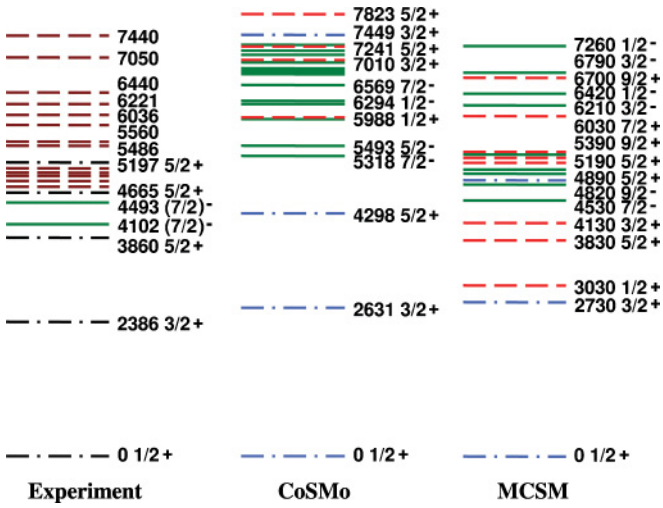

FIG. 3. (Color online) First column: experimental levels in ^{35}P from this and previous works. Measured positive-parity states are in black (dashed-dotted line) [20,21], tentatively assigned negative-parity states in green (solid line) [24], and states of unknown spin and parity in brown (dashed line). Second and third columns: shell model results from CoSMo and MCSM calculations (see text for details). $0\hbar\omega$ excitations are in blue (dashed-dotted line), $1\hbar\omega$ in green (solid line), and $2\hbar\omega$ in red (dashed line). For simplicity, not all negative-parity states are labeled.

Results from the shell model code CoSMo [25,26] are given in the middle column of Fig. 3. We used the standard WBP interaction [27] with sd-shell, pf-shell, and sd-pf cross-shell interactions. The model contains interactions between $T = 0$ (n-p) and $T = 1$ (n-n, p-p) valence nucleons with a full diagonalization of the combined sd-pf shells. The model predicts the first three $0\hbar\omega$ positive-parity states $1/2^+$, $3/2^+$, and $5/2^+$ in the correct sequence with the approximate energies. Experimental results suggest two more $5/2^+$ [20,21] states at 4665(3) and 5197(8) keV. To account for these states, $2\hbar\omega$ excitations into the pf shell are essential. The $5/2^+$ $2\hbar\omega$ states are predicted at 7241 and 7823 keV in this shell model, significantly higher than observed experimentally. Additionally, the calculation predicts a high density of $1\hbar\omega$ excitations above 6.5 MeV. From experimental data, the higher density of states is apparent already at ~4.5 MeV, and although no spin and parity information is available for the states above 4.5 MeV, it is reasonable to assume that most originate from $1\hbar\omega$ excitations, considering that almost all of the predicted positive-parity states are accounted for. Both the $1\hbar\omega$ and $2\hbar\omega$ states are predicted to lie higher in excitation energy than experimentally observed, a clear shortcoming of the calculations.

The last column of Fig. 3 shows results from the MCSM [28–30] calculations using the sd-pf-M interaction. Here, the MCSM calculation operated in the same model space as CoSMo, albeit with a different interaction; however, it had the additional capability to include mixing between different intruder configurations (e.g., $0\hbar\omega$, $2\hbar\omega$, $4\hbar\omega$) leading to additional modification of single-particle energies. This model has been very successful in describing nuclear properties far from stability, particularly for nuclei transitioning to, or located within, the island of inversion. Although states dominated by $0\hbar\omega$ configurations are comparable to both shell model results, the MCSM states of mixed configurations are lower in energy. Generally, the MCSM predicts level densities comparable to experimental observations.

Experimentally, five states have been identified to be of positive-parity generated from $0\hbar\omega$ and $2\hbar\omega$ excitations (black dashed-dotted lines in Fig. 3). Comparing the levels in Fig. 3, it is apparent that the MCSM calculation predicts the $2\hbar\omega$ excitations (red dashed line) to be significantly lower in energy than CoSMo calculations. With the lowering of the $2\hbar\omega$ states, all three observed $5/2^+$ states have analog states predicted within a few hundred keV in the MCSM calculations. CoSMo calculations using standard sd-pf single-particle energies (s.p.e.) predict the presence of two $2\hbar\omega$ $5/2^+$ states above 7 MeV. This is an indication that the shell gap between the sd and pf shells used in the model calculations has been somewhat overestimated. When the sd-pf shell gap is reduced by 1.2 MeV (all fp s.p.e. are simultaneously lowered relative to the sd s.p.e.), the agreement with measured states is improved significantly. In particular, the observed $5/2^+$ states at 4.6 and 5.2 MeV are now predicted at approximately the correct excitation energies. The predicted $1\hbar\omega$ level density then also appears at similar excitation energies compared to measurement.

$0\hbar\omega$ excitations are independent of the sd-pf shell gap and can be compared more directly in the two theoretical approaches. One striking difference between the calculations is the nature of the first $5/2^+$ state. CoSMo predicts this $5/2^+_1$ level to be 100% $0\hbar\omega$ (spherical), whereas MCSM calculations suggest the first $5/2^+$ state to have 83% $2\hbar\omega$ (deformed) and only 10% $0\hbar\omega$ (spherical) components. In addition, the $1/2^+_2$ $2\hbar\omega$ bandhead is predicted at an excitation energy of 3030 keV in MCSM (84% $2\hbar\omega$) and 5988 keV in CoSMo calculations. The "spherical" $5/2^+_2$ state is located at 4890 keV in MCSM, and even this state is highly mixed, with 55% $0\hbar\omega$ and 43% $2\hbar\omega$ components. Overall, MCSM calculations provide the better description of ^{35}P, and they also perform better in locating the $2\hbar\omega$ 0^+ bandhead in ^{36}S, which is observed at 3346(4) keV [12] and calculated at 3430 keV.

TABLE I. Calculated (MCSM) transition energies (E_γ) and decay strengths $B(E2)\uparrow$ between the first-excited $2\hbar\omega$ states to the $0\hbar\omega$ ground states and $2\hbar\omega$ bandheads in ^{35}P and ^{34}Si. $I_i^\pi \rightarrow I_f^\pi$ indicates the spin and parity for the initial and final state. BR is the extracted branching ratio.

Nucleus	$I_i^\pi \rightarrow I_f^\pi$	E_γ (keV)	$B(E2)\uparrow$ (e^2 fm^4)	BR (%)
^{35}P	$5/2^+_1 \rightarrow 1/2^+_1$	3830	41	99.9
^{35}P	$5/2^+_1 \rightarrow 1/2^+_2$	800	147	0.1
^{34}Si	$2^+_1 \rightarrow 0^+_1$	2900	74	99.2
^{34}Si	$2^+_1 \rightarrow 0^+_2$	830	317	0.8

The MCSM calculations predict low-lying $2\hbar\omega$ $1/2^+_2$ and 0^+_2 bandheads in ^{35}P and ^{34}Si at 3030 and 2070 keV, respectively, connected by a weak γ branch to the next higher lying intruder state. Calculated transition energies and $B(E2)$ values between the ^{35}P $5/2^+_1$ (^{34}Si 2^+_1) state and the $0\hbar\omega$ ground state and $2\hbar\omega$ bandhead are given in Table I. The predicted branching ratios BR($2\hbar\omega/0\hbar\omega$) are given in the last column; where, for ^{35}P, BR($2\hbar\omega/0\hbar\omega$) $= I(5/2^+_1 \rightarrow 1/2^+_2)/I(5/2^+_1 \rightarrow 1/2^+_1)$. Summed spectra double-gated on transitions feeding the $5/2^+_1$ 3860 keV state in ^{35}P and the 2^+_1 3326 keV state in ^{34}Si were used to search for a γ branch to the $2\hbar\omega$ bandhead. No decays to the $2\hbar\omega$ bandheads were observed either for ^{35}P or ^{34}Si in these data. Experimental BR($2\hbar\omega/0\hbar\omega$) limits were derived for both ^{35}P and ^{34}Si from the double-gated spectra and are shown in Fig. 4 as a function

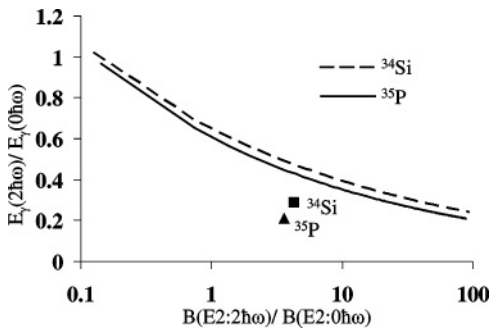

FIG. 4. Branching ratio limit for decays to predicted $2\hbar\omega$ bandheads in ^{35}P and ^{34}Si plotted as a function of the E_γ and $B(E2)$ ratios (see text for details). Predicted (MCSM) values are shown for ^{35}P and ^{34}Si. Values of E_γ and $B(E2)$ ratios that lie above the lines are excluded from this work.

of the ratio of the γ-ray energies, $E_\gamma(2\hbar\omega)/E_\gamma(0\hbar\omega)$, and the ratio of transition strengths, $B(E2:2\hbar\omega)/B(E2:0\hbar\omega)$. The curves correspond to a 2σ peak limit, obtained from the fluctuations in the gated, background-subtracted spectra; the limits include the energy-dependent γ-ray efficiencies and peak widths. Values of E_γ and $B(E2)$ ratios that lie above the lines are excluded from this work. We note the known 1473 keV $5/2_1^+$ to $3/2_1^+$ transition in ^{35}P corresponds to a 12% branch and is observed with an intensity of $\sim 3\sigma$ in these data. The MCSM calculated branching ratios are located in the region below the experimental sensitivity in this work and cannot be excluded.

Further experimental work is required to establish the excitation energy of the $2\hbar\omega$ bandheads. The $5/2_3^+$ level has a similar percentage of $2\hbar\omega$ component (according to MCSM calculations) as the $2\hbar\omega$ bandhead. So far only the $(d,^3\mathrm{He})$ reaction has been successful in populating the $5/2_2^+$ and $5/2_3^+$ states in ^{35}P, although no γ-decay information was available from these experiments [20,21]. It would be interesting to perform a $(d,^3\mathrm{He})$ experiment to search for the $5/2_3^+ \rightarrow 1/2_2^+$ γ transition, which has a 42% predicted branching ratio.

In summary, the structure of neutron-rich sd-pf shell nuclei in the mass $A \sim 35$ region has been investigated through nucleon transfer experiments using the ^{208}Pb(^{36}S, $X\gamma$) reaction at 230 MeV. The level scheme of the $N = 20$ nucleus ^{35}P was significantly expanded above an excitation energy of 4.3 MeV. The measurements were compared against calculations from the m-scheme shell models CoSMo and MCSM. The newly observed states appear to be mainly due to $1\hbar\omega$ excitations. The MCSM provides a good description of the observed $2\hbar\omega$ excitation spectrum. The location of the predicted lowest $2\hbar\omega$ excitations in ^{34}Si and ^{35}P could not be determined. The calculated branching ratios for these transitions lie below the sensitivity of the experimental data. Their experimental determination would provide valuable input to understanding how the sd-pf shell gap evolves for systems along the $N = 20$ isotonic chain.

The authors thank the operations staff of the ATLAS facility at Argonne National Laboratory. This work was supported by the Director, Office of Science, Office of Nuclear Physics, of the U.S. Department of Energy under Contract No. DE-AC02-05CH11231 (LBNL) and DE-AC02-06CH11357 (ANL). Part of this work was performed under the auspices of the U.S. Department of Energy Lawrence Livermore National Laboratory under Contract DE-AC52-07NA27344.

[1] J. Dobaczewski *et al.*, Prog. Part. Nucl. Phys. **59**, 432 (2007).
[2] C. Détraz *et al.*, Nucl. Phys. **A394**, 378 (1983).
[3] T. Motobayashi *et al.*, Phys. Lett. **B346**, 9 (1995).
[4] V. Chisté *et al.*, Phys. Lett. **B514**, 233 (2001).
[5] C. Thibault *et al.*, Phys. Rev. C **12**, 644 (1975).
[6] B. V. Pritychenko *et al.*, Phys. Rev. C **63**, 011305(R) (2000).
[7] Y. Yanagisawa *et al.*, Phys. Lett. **B566**, 84 (2003).
[8] E. K. Warburton, J. A. Becker, and B. A. Brown, Phys. Rev. C **41**, 1147 (1990).
[9] Y. Utsuno T. Otsuka, T. Mizusaki, and M. Honma, Phys. Rev. C **60**, 054315 (1999).
[10] F. Nowacki and A. Poves, arXiv:0712.2936v1 (2007).
[11] T. Otsuka, T. Suzuki, R. Fujimoto, H. Grawe, and Y. Akaishi, Phys. Rev. Lett. **95**, 232502 (2005).
[12] J. W. Olness *et al.*, Phys. Rev. C **3**, 2323 (1971).
[13] W. Mittig *et al.*, Eur. Phys. J. A **15**, 157 (2002).
[14] S. Nummela *et al.*, Phys. Rev. C **63**, 044316 (2001).
[15] J. Enders *et al.*, Phys. Rev. C **65**, 034318 (2002).
[16] N. Iwasa *et al.*, Phys. Rev. C **67**, 064315 (2003).
[17] M. W. Simon *et al.*, Nucl. Instrum. Methods Phys. Res. **A452**, 205 (2000).
[18] I.-Yang Lee, Nucl. Phys. **A520**, c641 (1990).
[19] N. A. Orr *et al.*, Nucl. Phys. **A477**, 523 (1988).
[20] C. E. Thorn, J. W. Olness, E. K. Warburton, and S. Raman, Phys. Rev. C **30**, 1442 (1984).
[21] S. Kahn *et al.*, Phys. Lett. **B156**, 155 (1985).
[22] J. P. Durfour *et al.*, Z. Phys. A **324**, 487 (1986).
[23] P. Baumann *et al.*, Phys. Lett. **B228**, 452 (1989).
[24] E. K. Warburton and J. A. Becker, Phys. Rev. C **35**, 1851 (1987).
[25] A. Volya and V. Zelevinsky, Phys. Rev. Lett. **94**, 052501 (2005).
[26] A. Volya and V. Zelevinsky, Phys. Rev. C **74**, 064314 (2006).
[27] E. K. Warburton and B. A. Brown, Phys. Rev. C **46**, 923 (1992).
[28] M. Honma, T. Mizusaki, and T. Otsuka, Phys. Rev. Lett. **75**, 1284 (1995).
[29] T. Otsuka, M. Honma, and T. Mizusaki, Phys. Rev. Lett. **81**, 1588 (1998).
[30] T. Otsuka, T. Mizusaki, and M. Honma, J. Phys. G **25**, 699 (1999).